Investigation into ion edge temperature behaviour using CER spectroscopy at DIII-D

1995 Nucl. Fusion 35 347

(http://iopscience.iop.org/0029-5515/35/3/I08)

INVESTIGATION INTO ION EDGE TEMPERATURE BEHAVIOUR USING CER SPECTROSCOPY AT DIII-D

W. MANDL*, K.H. BURRELL, R.J. GROEBNER, J. KIM,
R.P. SERAYDARIAN, M.R. WADE**, J.T. SCOVILLE
General Atomics,
San Diego, California,
United States of America

ABSTRACT. Measurements with high spatial resolution in the neighbourhood of the separatrix show edge ion temperatures in the 1–2 keV range, exceeding the electron temperature substantially, in neutral beam heated H mode discharges on DIII-D. Charge exchange recombination (CER) spectroscopy on light ions such as He^{2+} and C^{6+} is used to measure ion temperature, ion density and poloidal and toroidal plasma rotation profiles. Near the separatrix the spatial resolution of the measurements is a few millimetres. The scale length for the edge ion temperature gradient is found to be about one third of the poloidal gyroradius, i.e. a factor of 2 to 3 longer than the neoclassical scale length. The electron temperatures at the plasma edge are substantially ($\simeq$1 keV) lower than the ion temperatures. Outside the separatrix, T_i is also found to be higher than T_e. We investigate the power balance globally and locally at the plasma edge. It is found that the high heat transfer from the ions to the electrons, just inside the separatrix, can be balanced by local ion heating due to neutral beam absorption.

1. INTRODUCTION

The control of boundary conditions and the improvement of the energy confinement are among the main goals of controlled nuclear fusion research. A sufficiently hot plasma edge, making the plasma near the separatrix nearly collisionless, helps to direct particle and heat exhaust into the divertor by reducing radial diffusivity. In addition, low edge collisionality might be an important condition for obtaining H mode confinement in tokamak discharges [1, 2]. The observed edge ion temperatures have far reaching implications for fusion reactivity, power handling, wall erosion and impurity production in reactor conditions. An enhanced flux of highly energetic particles to the first wall has profound implications for future limiter and divertor designs.

In this paper we concentrate on hot ion H mode discharges. These discharges develop steep temperature and density gradients at the plasma edge, and ion temperatures are in the range of 1–2 keV at the separatrix. Similar results have been observed at JET, where the edge temperature gradient, however, could not be resolved [3]. The good spatial resolution of the CER system at DIII-D enables highly resolved edge gradient measurements in the vicinity of the separatrix. We investigate the collisionality regime in the plasma edge region and compare the measured edge temperature gradients with predictions made by neoclassical theory [4] for the collisionless case.

Electron temperatures, measured by Thomson scattering, are substantially lower than ion temperatures in the vicinity of the last closed magnetic flux surface and even beyond. Ion–electron heat exchange is therefore taking place at a large rate. A neutral beam attenuation calculation, based on measured temperature and density profiles, allows us to evaluate the local contributions to ion and electron heating from the energy loss of ionized, slowing down beam particles. The local power balance is derived, identifying the major heat transfer channels. This analysis shows that the power input to the plasma is quite sufficient to sustain the measured temperature difference.

2. THE EXPERIMENT

In shots 77 283–77 317 single-null divertor discharges were produced in a vessel with unboronized, all graphite walls. We choose to concentrate on shot 77 283 and a repeat shot (77 284) with similar parameters. Plasma breakdown occurred in helium prefill. Prior to neutral beam injection, a target density of $n_e = 1.2 \times 10^{19}$ m^{-3} was maintained by the density

Permanent affiliations:
* Max-Planck-Institute for Plasma Physics/Euratom Association, Garching, Germany.
** Oak Ridge National Laboratory, Oak Ridge, Tennessee, United States of America.

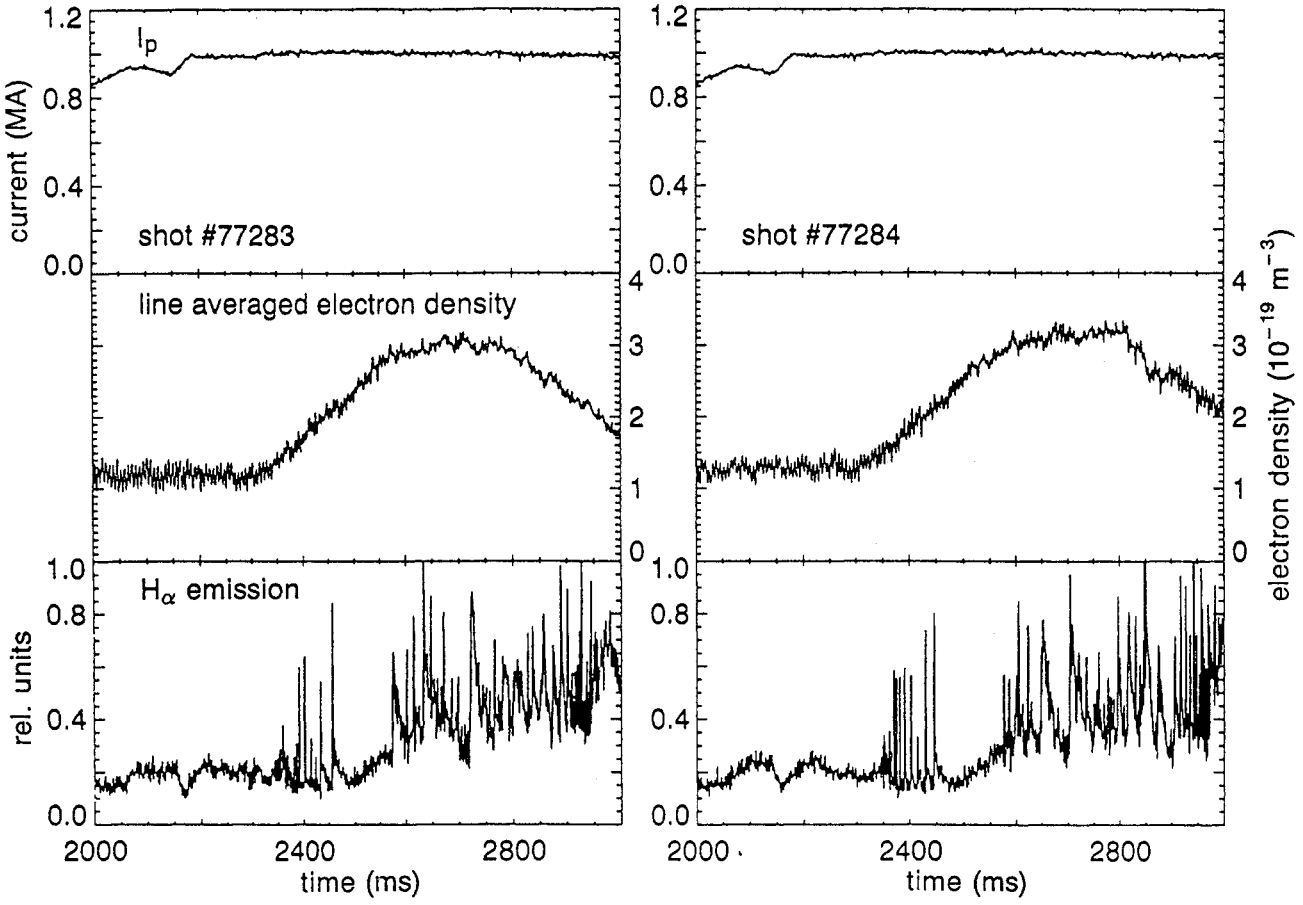

FIG. 1. Time traces showing the plasma current, the line averaged electron density as measured by the CO_2 interferometer and the H_α edge emission for repeat shots 77283 and 77284. Neutral beam injection starts at 2300 ms. Both shots show an ELMy L to H mode transition at about 2360 ms. The CER diagnostic was used to record the helium spectra during shot 77283 and during shot 77284 the carbon spectra were recorded.

feedback control system, which was also using helium. The vacuum magnetic field was 2 T at the magnetic axis and the total plasma current I_P was 1 MA. Both discharges show a dithering L to H mode transition approximately 50 ms after the start of neutral beam heating at 2300 ms. The discharges exhibit edge localized modes (ELMs) for about 100 ms right after the L to H mode transition, and after an ELM-free period of a little over 100 ms ELMing starts again (Fig. 1).

The divertor cryopump was utilized in an attempt to remove the cold deuterium influx at the edge, which recycles from the walls and drifts in from the neutral beam ducts. Four neutral beams, injecting deuterium, were modulated (5 ms on, 5 ms off) to facilitate the CER analysis. The injected power was kept constant by modulating groups of two beams out of phase with respect to each other, in order to avoid ELMs locking to the beam modulation. One more beam was injecting deuterium continuously to help produce an L to H mode transition. The beams introduce deuterons and electrons into the discharge. Electrons deposited by the ionization of the injected fast deuterium atoms replace the electron inventory on the time-scale of the electron particle confinement time (0.2–0.4 s). The beam fuelling dilutes the initially almost pure helium discharge substantially. The helium concentration n_{He}/n_e in the plasma centre is diluted to about 10% a few hundred milliseconds after the onset of neutral beam injection (Fig. 2). Simultaneously, wall erosion by the plasma causes carbon influx. A carbon concentration of $n_C/n_e \approx 1.5\%$ is reached at the edge (Fig. 3). The analysis method used to extract helium and carbon densities from the spectroscopic data is discussed in the next section.

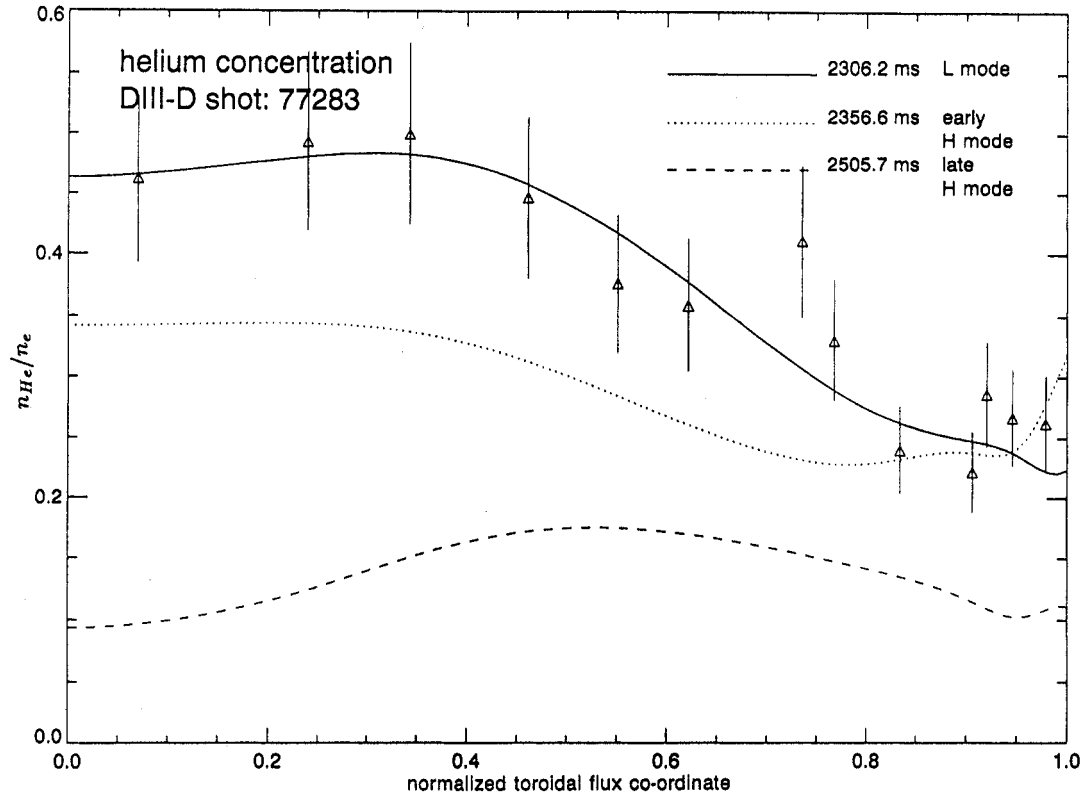

FIG. 2. Evolving helium concentration profile. The time slices are taken 6.2, 56.6 and 205.7 ms after the start of neutral beam heating. Individual measurements, obtained from vertical viewing chords of the CER system, are shown for the first time slice only. The error bars reflect estimated statistical uncertainties.

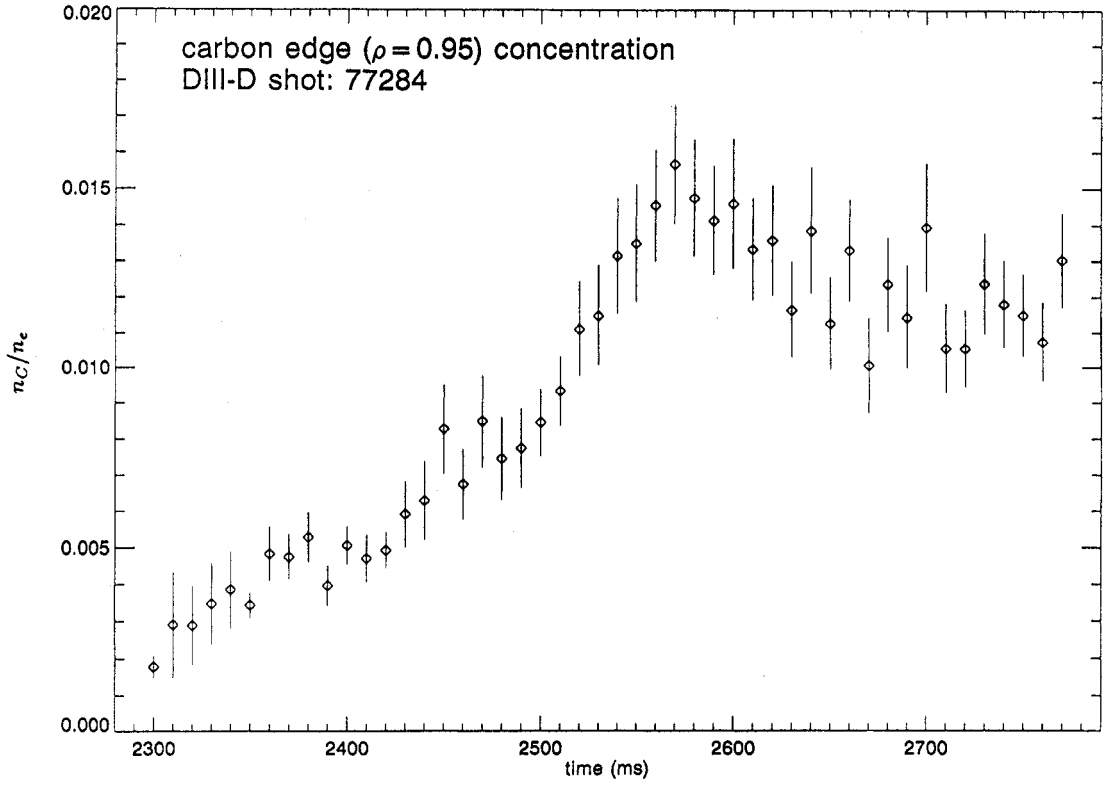

FIG. 3. Evolving carbon concentration near the separatrix as a function of time.

3. CER MEASUREMENTS

CER spectroscopy is routinely used in many fusion experiments [5–8] to determine the local ion temperature T_i as well as toroidal and poloidal plasma rotation velocities (v_t, v_p). Light from charge exchange reactions

$$Z^{Z+} + D^0 \Rightarrow Z^{(Z-1)+\star} + D^+ \quad (1)$$

$$Z^{(Z-1)+\star} \Rightarrow Z^{(Z-1)+} + \gamma \quad (2)$$

between fully stripped impurity ions Z^{Z+} and fast injected deuterium atoms D^0 is gathered along viewing lines intersecting the neutral atom beams. At DIII-D, 16 horizontal and 16 vertical viewing chords allow the simultaneous observation of 32 radial locations (Gohil et al. 1992). A time resolution of 2 ms in the bulk plasma and of 0.5 ms at the plasma edge can be achieved. The radial spacing for T_i is 3 cm near the plasma centre and as fine as 3 mm in the vicinity of the separatrix. The radial spacing for rotation measurements is twice as large. Thus, the CER diagnostic at DIII-D is a very versatile tool. It covers nicely the bulk plasma and has adequate radial resolution at the plasma edge, where the steepest temperature gradients occur.

CER measurements have been conducted on He II (λ = 486 nm) and C VI (λ = 529 nm) spectral lines. Helium profiles have been measured over the whole minor radius in shot 77 283, and in repeat shot 77 284 the outer half of the profile data was obtained from measurements on carbon spectral lines. Central carbon data could not be obtained because the signal was generally too weak.

The recorded spectra generally consist of a superposition of bremsstrahlung, some passive plasma emission from the edge and the active CER signal. We are extracting the CER component of the signal by subtracting background spectra, which were recorded during the periods when the modulated neutral beams were off. A least squares method is then applied to fit a Gaussian line shape, convolved with the instrumental function, to the measurement. The Doppler broadening and Doppler shift of the emitted spectral line are determined from the fit. They are interpreted as the effects of temperature and mean velocity of the displaced Maxwellian energy distribution of the plasma ions. While significantly different poloidal rotation velocities have been found for the main ions and the impurity ions, the T_i profiles are the same within the error bars of our measurements [10].

The impurity ion density n_Z is determined from the absolutely calibrated line intensity Φ_{CER}. The photon flux Φ_{CER} is proportional to the local ion density n_Z and the neutral beam particle density n_b,

$$\Phi_{CER} = \frac{n_Z}{4\pi} \sum_{i=}^{1,\frac{1}{2},\frac{1}{3}} q^i_{CX} \int n^i_b \, d\ell \quad (3)$$

In the deuterium neutral beams three energy species are present, corresponding to D^+, D_2^+ and D_3^+ in the positive ion source of the injector. We therefore have to sum over the full, half and third energy populations of the neutral beam which contribute ≈51, 31 and 18%, respectively, of the total NB power at DIII-D. The determination of n_Z depends on the neutral beam attenuation, which is affected strongly by the n_e profile and weakly by T_e and Z_{eff}. Effective cross-sections for charge exchange and neutral beam attenuation, derived from fundamental cross-sections with a collisional radiative model, are readily available from the JET atomic database ADAS[1]. T_e and n_e profiles from Thomson scattering and CO_2 interferometry [11, 12] are used to calculate the beam penetration. The Z_{eff} profile is obtained self-consistently from CER measurements on the main impurity ions He^{2+} and C^{6+} and from n_e, using its definition.

$$Z_{eff} = 1 + \sum_{Z>1} \frac{n_Z}{n_e}(Z^2 - Z) \quad (4)$$

The Z_{eff} profile obtained from CER measurements and n_e agrees with central values obtained from Abel inverted bremsstrahlung. It is, however, not sensitive to edge line radiation, which apparently causes the Abel inverted measurement to give too high a value at the edge in these helium plasmas.

The line integration in Eq. (3) is across the beam profile, along the individual CER viewing lines. The impurity ion density n_Z is assumed to be constant over the intersection volume between neutral beam and line of sight. The measurements are spline fitted to obtain smooth radial density profiles. Statistical errors are typically in the 10–20% region. Systematic errors originating from uncertainties in the multi-Gauss fit procedure, the calibration and the beam parameters are, however, difficult to estimate and can in some cases be as large as 50%.

In the case of helium spectra, the CER signal consists of the prompt, localized recombination radiation and a noticeable portion of the total signal which is

[1] ADAS is an interactive *a*tomic *d*ata and *a*pplications *s*tructure containing both fundamental and derived cross-section data, developed by H.P. Summers at JET to provide atomic data for plasma diagnostics.

ascribed to additional, non-localized, delayed emission. This delayed emission is assumed to be due to a plume of thermal, singly charged He^+ ions which have been created in the charge exchange process between fully ionized plasma ions and the injected fast neutrals [13, 14]. The plume particles follow the magnetic field lines and continue radiating, mainly owing to electron impact excitation, until they are fully ionized again. For the geometry at DIII-D, the plume effect is most prominent for the horizontal part of the CER system. Plume signals from flux surfaces outside the nominally observed locations mainly contribute. This contribution is characterized by a lower temperature and a Doppler shift that is different from the Doppler shift of the prompt signal. It can therefore be separated out and accounted for by introducing extra Gaussian components into the least squares fit procedure. The plume effect makes helium signals difficult to analyse and introduces a significant chance of systematic errors. Cross checks between temperature measurements from the horizontal system and from the vertical system, which is less affected by the plume effect, are conducted routinely to detect systematic errors.

4. EDGE ION TEMPERATURES AND EDGE TEMPERATURE GRADIENTS

An increasing edge ion temperature (Fig. 4) leads to a reduction in collisionality at the separatrix, the last closed flux surface. Steepening edge temperature and density gradients (Fig. 5) are observed shortly after the L to H mode transition, indicating the manifestation of a transport barrier. Gradients in the electron temperature T_e at the plasma edge are similar to T_i gradients during the period of ELM-free H mode. T_e at the separatrix, however, is lower than T_i by more than a factor of 2. Outside a normalized minor radius of $\rho = 1.1$, T_e is indistinguishable from zero by Thomson scattering.

The variation in magnetic field strength between the inner side ($B = B_{max}$) and the outer side ($B = B_{min}$) of the torus causes particles with too small a velocity component parallel to the magnetic field to undergo a magnetic mirror reflection as they move into the region of higher field. At the separatrix, a dominant fraction of the confined ions fulfils the mirror condition,

$$(v_{\|0}/v_{\perp 0})^2/(B_{max}/B_{min}) - 1$$

and is therefore trapped in banana orbits. $v_{\|0}$ and $v_{\perp 0}$ are, respectively the velocity components parallel and perpendicular to the magnetic field at the location of weakest magnetic field on the particle trajectory. Collisions cause these particles to diffuse in velocity space on the time-scale of the classical collision time τ_{coll}. Since τ_{coll} pertains to angle scattering of roughly 90°, the detrapping time will be $\tau_{detrap} = \tau_{coll}(\Delta\theta)^2$ [15], where

$$\Delta\theta = \sqrt{(B_{max} - B_{min})/B_{min}}$$

is the opening angle of the trapping cone in velocity space. Figure 6 shows τ_{detrap} for carbon ions in a dominantly deuterium edge plasma at $\rho = 0.95$,

$$\tau_{detrap} = 12\pi^{3/2}\frac{\epsilon_0^2 m_C^{1/2} T_i^{3/2}}{n_D Z_D^2 Z_C^2 e^4 \ln\Lambda}\frac{B_{max} - B_{min}}{B_{min}} \quad (5)$$

The banana regime is established at the plasma edge when the bounce time τ_{bounce},

$$\tau_{bounce} = qR_0\sqrt{\frac{R_0}{r}\frac{m_C}{T_i}} \quad (6)$$

which is needed to complete one banana orbit, is much shorter than τ_{detrap}. In Eq. (6) a large aspect ratio, and a circular plasma cross-section are assumed. The bounce time as shown in Fig. 6, which has been calculated using Eq. (6) is therefore only approximate. Figure 6 shows that carbon ions at the plasma edge, which have been utilized for the temperature measurement, enter into the banana regime ($\nu_{*i} \equiv \tau_{bounce}/\tau_{detrap} < 1$) shortly after the L to H mode transition, where the step length for diffusion processes is the banana width, i.e. one ion poloidal gyroradius $\rho_{ip} = \sqrt{2T_i m_i}/eB_p$. In the collisionless case, changes in the ion temperature and density are therefore expected to take place on a radial scale of ρ_{ip}. The values of ν_* for deuterium and helium are smaller by a factor of $(Z_D/Z_C)^2$ or by $(Z_{He}/Z_C)^2$, respectively. Deuterium and helium ions are therefore also found to be in the banana regime.

Neoclassical theory of ion transport [15] predicts in the collisionless case that the ion temperature gradient $\partial T_i/\partial r$ at the separatrix is proportional to the ion temperature T_i and inversely proportional to the ion poloidal gyroradius and the inverse aspect ratio $\epsilon = r/R$ of the plasma,

$$\left(\frac{\partial T_i}{\partial r}\right)^{neo} = -T_i\frac{2.2}{\epsilon\rho_{ip}} \quad (7)$$

From Eq. (7) a neoclassical ion temperature scale length $T_i/(\partial T_i/\partial r)$ of about 5 mm is predicted for our measurements. This is resolvable given the 3 mm radial resolution of the CER edge diagnostic system. Figure 7 compares the measured edge carbon temperature gradient with the neoclassical value and with T_i/ρ_{ip}. Ion temperature comparisons have shown that

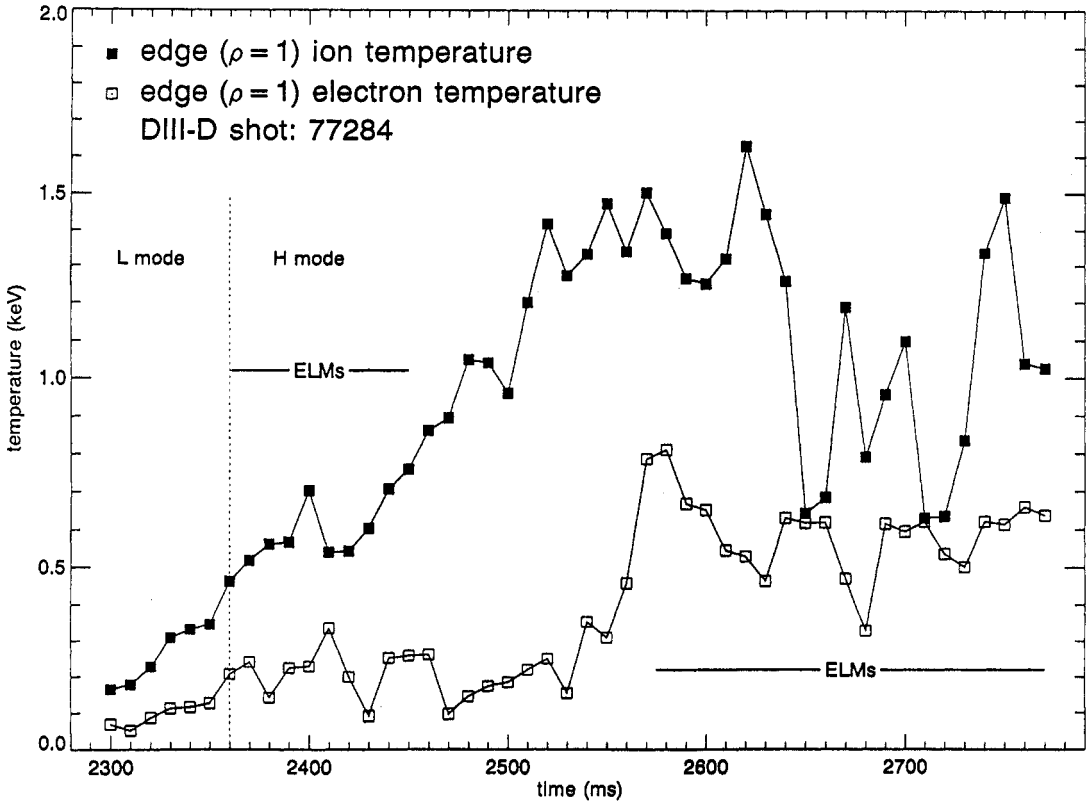

FIG. 4. Ion and electron edge temperatures at the separatrix location.

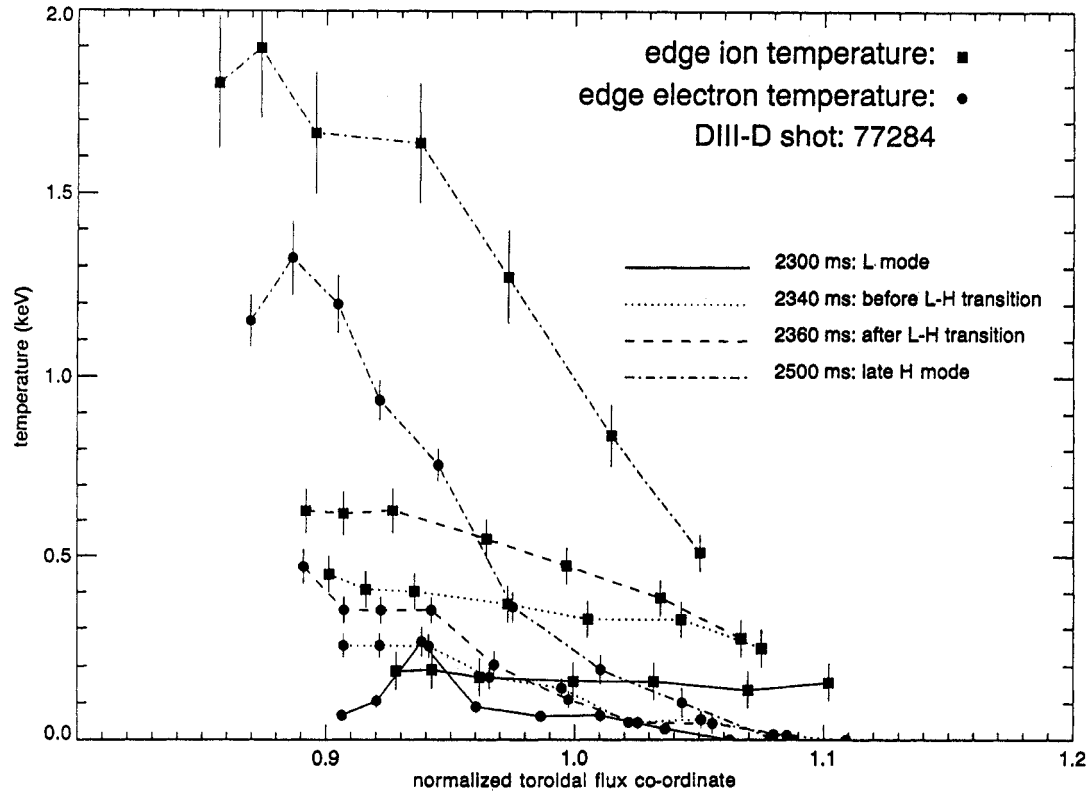

FIG. 5. Evolving edge ion and electron temperature profiles. Time slices are taken immediately after neutral beam turn on, 10 ms before and after the L to H mode transition and 200 ms after beam turn on.

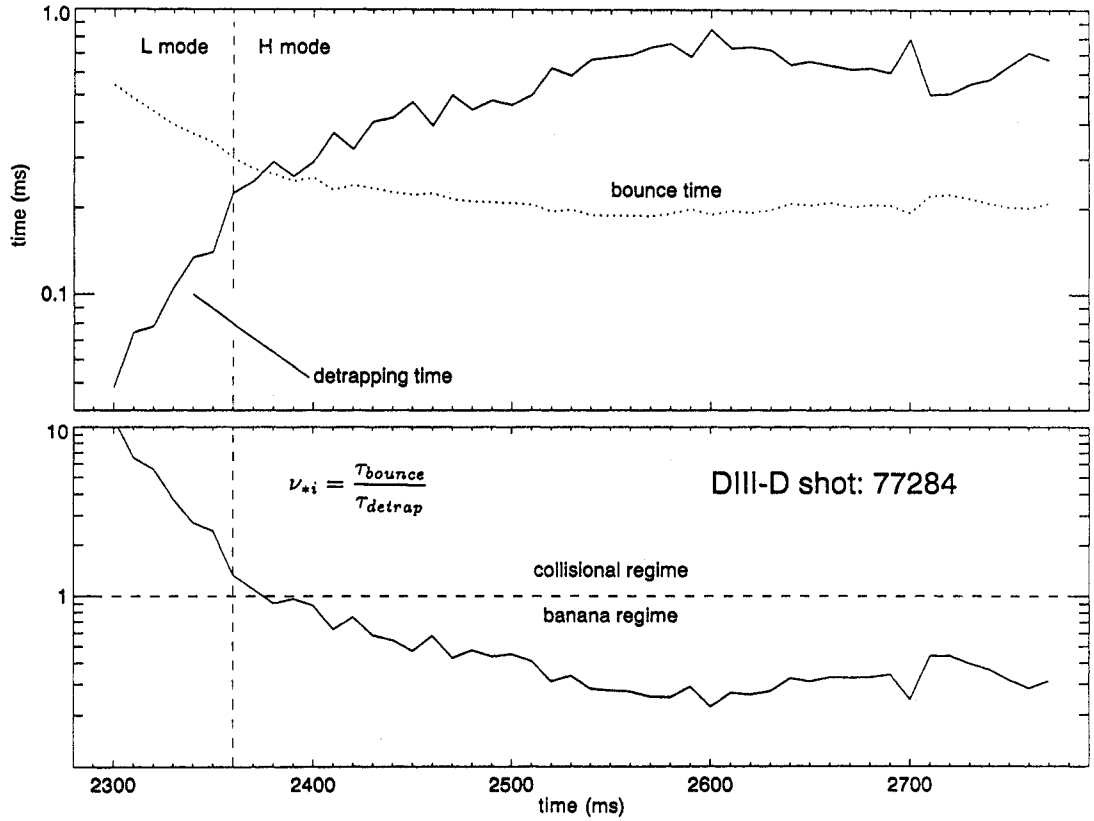

FIG. 6. Time evolution of τ_{bounce} and τ_{detrap} for carbon ions at $\rho = 0.95$. The banana regime is established at t = 2380 ms when the detrapping time becomes larger than the bounce time.

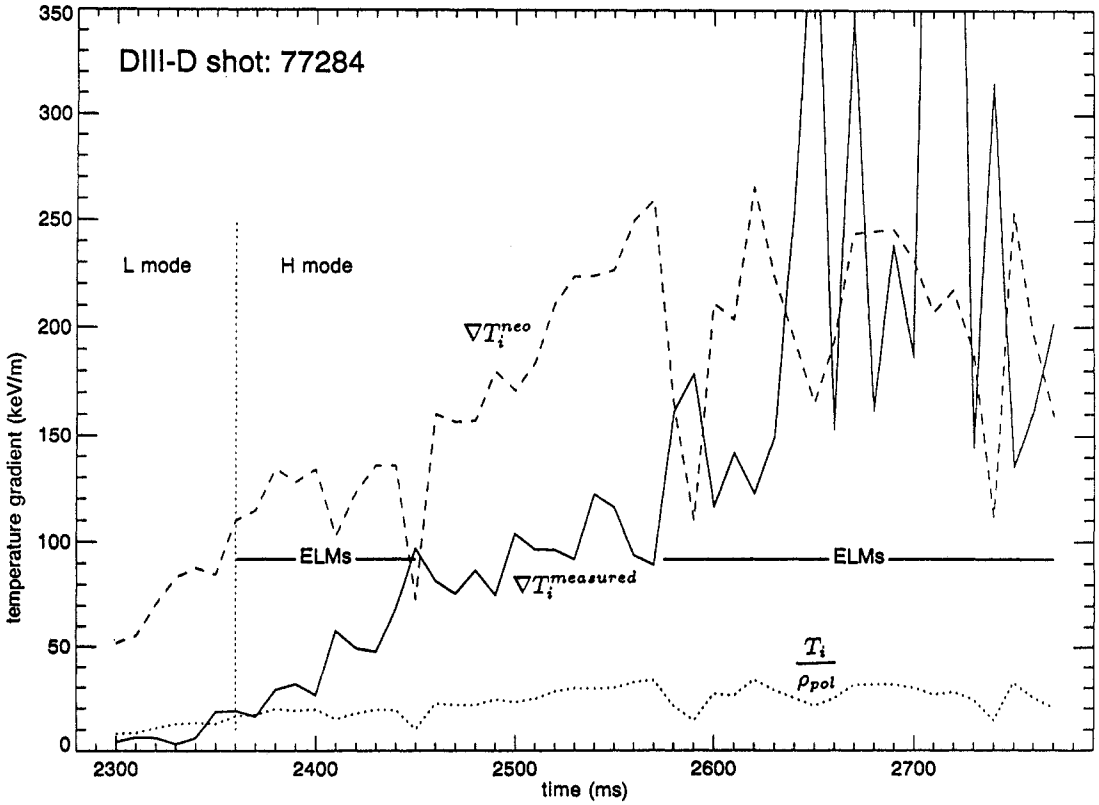

FIG. 7. Comparison between measured edge temperature gradient at the separatrix location, the gradients expected from neoclassical theory and T_i/ρ_{pol}.

all the ions have the same temperature. The temperature gradient displayed in Fig. 7 is taken as the steepest measured gradient within the edge region of $\rho = 0.9$–1. Our measurements indicate that the edge ion temperature gradient at the L to H mode transition is approximately T_i/ρ_{ip}. The factor $2.2/\epsilon$ in the neoclassical expression, Eq. (7), assumes values of between 6.4 and 8 for the data shown in Fig. 7. At the L to H transition, where also the transition from collisional to collisionless regime occurs, the neoclassically estimated edge T_i gradient is too steep by a factor of 6.4, compared with the measurements. For later time slices, during ELM-free H mode when the banana regime is clearly established, the measured gradient exceeds T_i/ρ_{ip} by a factor of 2 to 3 but is also a factor of 2 to 3 less than the neoclassical value. Only during late, heavily ELMing H mode are the neoclassical predicted gradient and the measured temperature gradient not in disagreement. The presence of strong ELMs, however, introduces large statistical errors in the 50% range into the temperature measurement. The temperatures for the calculation of the neoclassical value as well as for the T_i/ρ_{ip} scaling are taken at the separatrix ($\rho = 1$).

5. POWER BALANCE NEAR THE SEPARATRIX

Ion temperatures which are much in excess of the electron temperatures near the separatrix produce a large ion–electron energy exchange. We wish to discuss quantitatively the major heat fluxes that are involved in the power balance at the plasma edge.

The energy transfer between electrons and ions depends on τ_e, the collision time of the faster particles, the electrons. The difference in mass, however, makes the energy transfer inefficient. The ion–electron heat exchange time τ_{ie} between ions and electrons is therefore longer by a factor of $m_i/2m_e$ than τ_e [16].

At a typical electron edge density of $10^{19}\,m^{-3}$ and an electron temperature of 100 eV the heat exchange time

$$\tau_{ie} = \frac{3}{2}(2\pi)^{3/2}\frac{\epsilon_0^2 m_i T_e^{3/2}}{n_i m_e^{1/2} Z^2 e^4 \ln\Lambda} \tag{8}$$

is 4.4 ms in a pure deuterium plasma or a pure helium plasma ($\ln\Lambda \simeq 17$ is the Coulomb logarithm). A considerable heat flow Q_{ie} from the ions to the electrons has to be supported in order to maintain a temperature difference of up to 1 keV. The measured temperature and density profiles yield a heat transfer density,

$$\frac{dQ_{ie}}{dV} = \frac{3}{2}(T_i - T_e)\frac{n_e}{\tau_{ie}} \tag{9}$$

of up to 50 kW/m^3 at the edge (Fig. 8), if a pure deuterium plasma ($n_i = n_e$) is assumed. After substituting $n_i Z$ by n_e in Eq. (8) it becomes clear that even large concentrations of helium and carbon would have no influence on τ_{ie} since the ratio m/Z is the same for deuterium, helium and carbon. Since we have an edge helium concentration of about 10% during the time-slice shown in Fig. 8, the pure deuterium scenario is a good approximation. The total heat transfer Q_{ie} is found by integrating over the entire plasma volume V. It is about 747 kW, i.e. 11% of the total injected neutral beam power of 6.6 MW. The total heat transfer Q_{ie}^{edge} at the plasma edge, integrated between $\rho = 0.7$ and $\rho = 1$, is about 208 kW.

Ohmic heating in this 1 MA discharge is estimated to be about 6.5 kW/m^3 in the plasma centre and is negligible at the edge. The only auxiliary heating in these discharges is neutral beam heating. The neutral beams deposit approximately 950 kW in the edge region between $\rho = 0.7$ and $\rho = 1$. Fast ions, created by ionization of neutral beam atoms, are approximately confined to the flux surface on which the ionization occurred. These fast beam ions are thermalizing by ion and electron collisions. For monoenergetic ions the fraction of the neutral beam power per beam ion, which is contributing to ion and to electron heating is given by [16]:

$$P_{NBI}^{i} = 0.97 \times 10^{-16}\frac{n\sqrt{A_b}}{A_i\sqrt{E_b}} \tag{10}$$

$$P_{NBI}^{e} = 1.71 \times 10^{-18}\frac{nE_b}{A_b T_e^{3/2}} \tag{11}$$

The electron temperature T_e and the beam energy E_b are in keV, $n = n_i = n_e$ is in m^{-3}, and A_i and A_b are, respectively, the atomic mass numbers of plasma ions and beam particles. P_{NBI}^{i} and P_{NBI}^{e} are, respectively, heating powers to ions and electrons in keV/s. Numerical integration of the slowing down process, using Eqs (10) and (11) for the full, half and third energy fractions of the beams, gives the total ion and electron heating. The slowing down process is initially, at full beam energy, mainly heating the electrons. As the beam ions lose energy, more and more heating goes into the ions. Figure 9 shows the neutral beam heating energy deposition density profile dP_{NBI}/dV. The contributions to ion heating and electron heating are shown separately. The electrons are predominantly heated at the very edge of the plasma, where T_e is low. Neutral beam heating contributes about 520 kW to ion heating and 430 kW to electron heating in the plasma volume between $\rho = 0.7$ and the

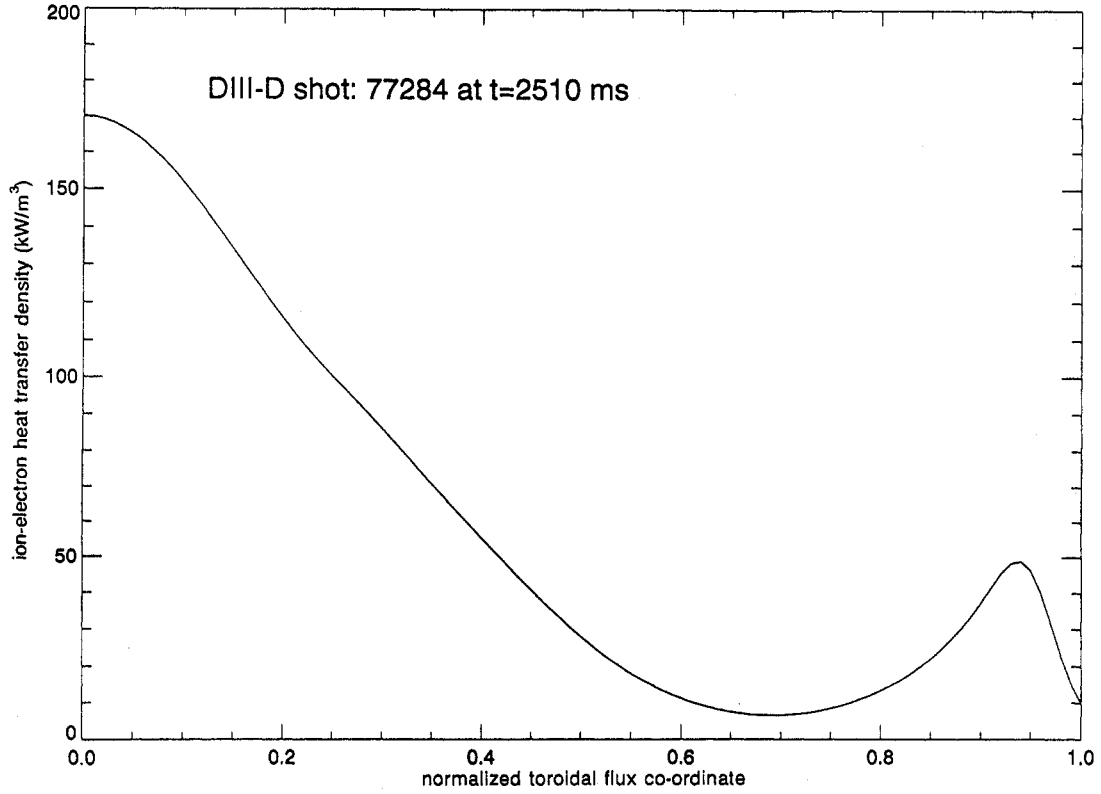

FIG. 8. The ion–electron heat transfer density during late H mode was derived from spline fitted measurements of temperature and density profiles.

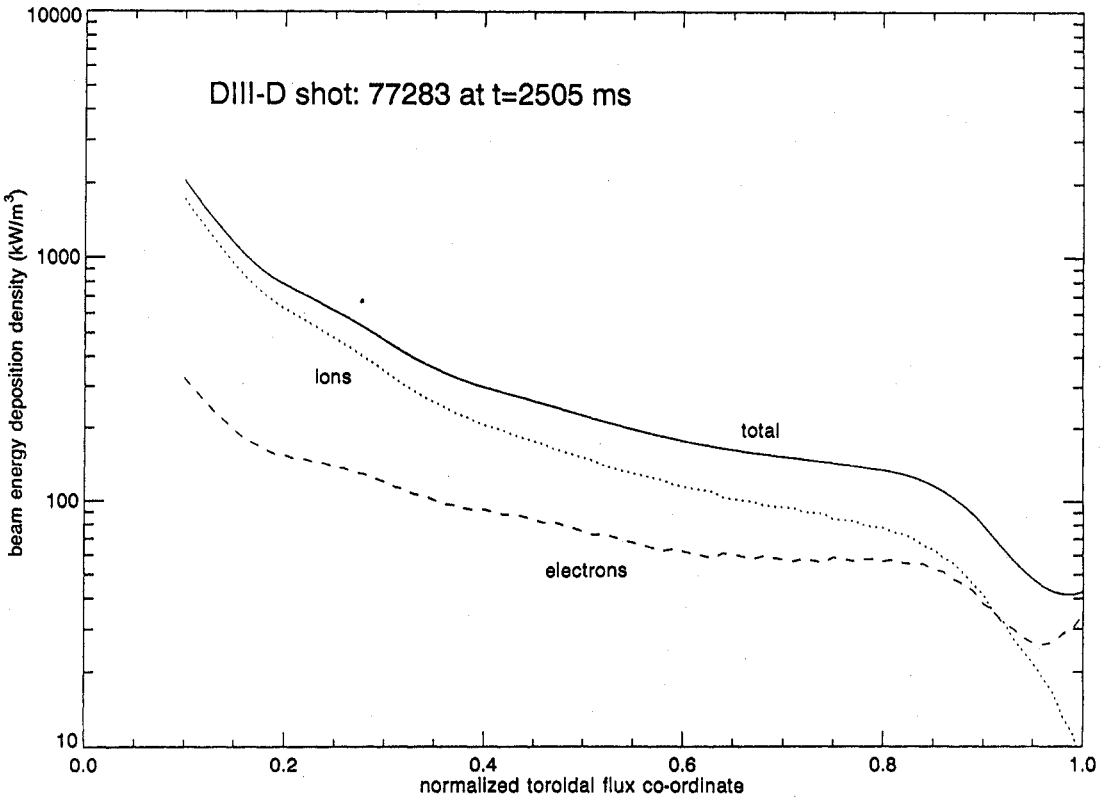

FIG. 9. Neutral beam heating energy deposition density profile. The fractions contributing to ion and electron heating are shown separately.

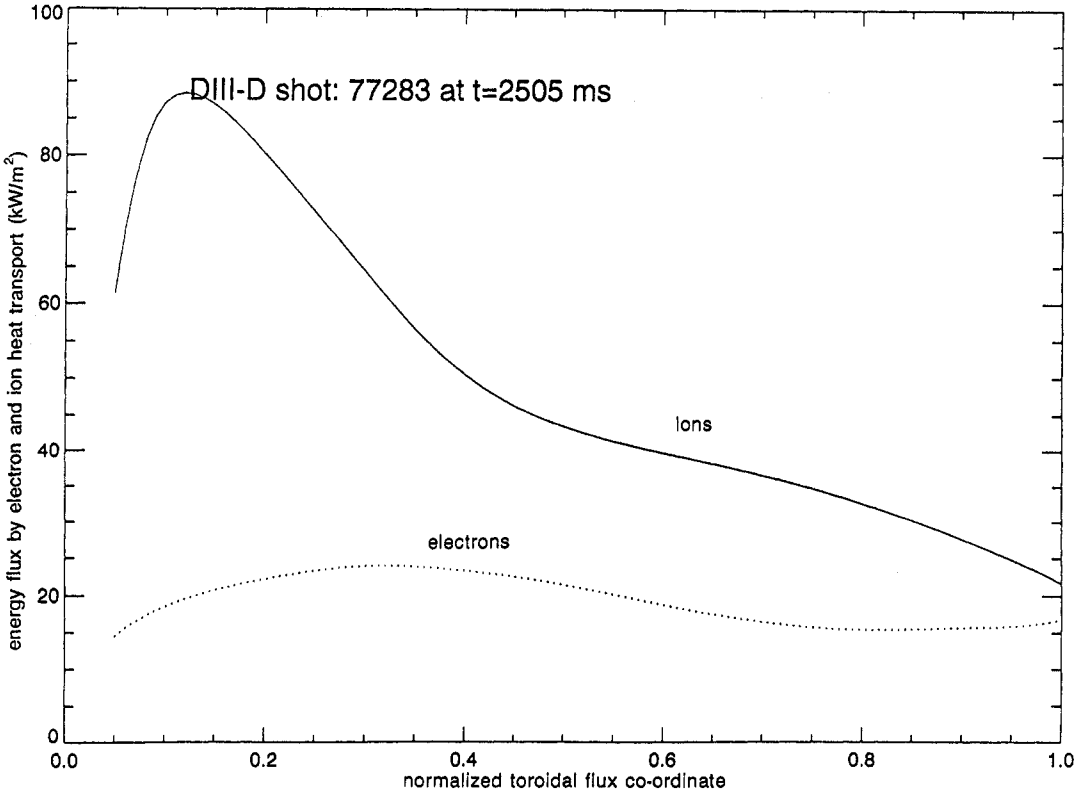

FIG. 10. Radial outflux of energy in the ion and electron channels by convective and conductive processes.

separatrix. Ion heating by neutral beam deposition is therefore large enough to compensate locally for the ion–electron heat transfer term. The total ion and electron heat fluxes P/S by conductive and convective processes (Fig. 10) are defined by

$$\left(\frac{P}{S}\right)^{\mathrm{i}} = \left(P^{\mathrm{i}}_{\mathrm{NBI}} - P_{\mathrm{ie}} - \frac{\partial W_{\mathrm{i}}}{\partial t}\right)\frac{1}{S} \tag{12}$$

$$\left(\frac{P}{S}\right)^{\mathrm{e}} = \left(P^{\mathrm{e}}_{\mathrm{NBI}} + P_{\mathrm{ie}} - P_{\mathrm{rad}} - \frac{\partial W_{\mathrm{e}}}{\partial t}\right)\frac{1}{S} \tag{13}$$

The radiation loss P_{rad} is obtained from Abel inversion of line integrated bolometer signals. The radiation density has an almost flat radial profile at an average value of 27 ± 3 kW/m^3. The time derivatives of the thermal energies of ions and electrons $\partial W_{\mathrm{i}}/\partial t$, $\partial W_{\mathrm{e}}/\partial t$ are taken into account. All powers are derived by integrating the power densities over the volume inside a flux surface with flux label ρ and area S. Figure 10 shows that the net energy flux, in the ion as well as in the electron channel, is positive, i.e. directed outwards, at all locations. The ion–electron energy exchange term can therefore be accommodated without violation of the global energy balance.

6. RESULTS AND CONCLUSIONS

Edge ion temperatures in excess of 1 keV at the separatrix location are reported. T_{i} is also found to be higher than T_{e} outside the separatrix. High ion temperatures at the scrape-off layer cause a flux of energetic particles into the loss areas, which will have profound implications for the power handling in plasma divertors in future fusion reactors. Theoretical approaches describing the plasma edge and scrape-off layer have to accommodate electron temperatures at the plasma edge that are substantially ($\simeq$1 keV) lower than the ion temperatures.

The large energy transfer from the ions to the electrons at $\rho \geq 0.9$, which is caused by the difference between electron and ion temperatures, is balanced by heat deposition from the neutral beam heating to the ions. It is also consistent with an overall positive global power balance.

The scale length for the edge ion temperature gradient $L_{T_{\mathrm{i}}} = T_{\mathrm{i}}/(\partial T_{\mathrm{i}}/\partial r)$ is about one poloidal gyroradius ρ_{p} at the transition from a collisional regime to the banana regime. It is two to three times shorter than ρ_{p} during ELM-free H mode, where the banana regime

is clearly established. That is, however, a factor two to three longer than the neoclassical scale length.

All in all, it can be concluded that the high ion edge temperatures and the very steep ion temperature gradients at the separatrix location, as observed at DIII-D, are well explained by standard heating and heat exchange mechanisms. The observed temperature gradients are consistent with neoclassical predictions.

ACKNOWLEDGEMENTS

We would like to thank M. von Hellermann and H.P. Summers at JET for providing us with atomic cross-section data for neutral beam attenuation and charge exchange processes. This is a report of work sponsored by the USDOE under Contract No. DE-AC03-89ER51114 and by the Commission of the European Communities under the Agreement for the Promotion of Staff Mobility.

REFERENCES

[1] WAGNER, F., et al., Phys. Rev. Lett. **49** (1982) 1408.
[2] SHAING, K.C., CRUME, E.C., Jr., Phys. Rev. Lett. **63** (1989) 2369.
[3] WEISEN, H., et al., Nucl. Fusion **31** (1991) 2247.
[4] HINTON, F.L., HAZELTINE, R.D., Rev. Mod. Phys. **48** (1976) 239.
[5] FONCK, R.J., et al., Appl. Phys. Lett. **42** (1983) 239.
[6] GROBENER, R.J., et al., Appl. Phys. Lett. **43** (1983) 920.
[7] ISLER, R.C., et al., Phys. Rev. A **24** (1981) 2701.
[8] WEISEN, H., et al., Nucl. Fusion **29** (1989) 2187.
[9] GOHIL, P., et al., in Fusion Technology (Proc. 14th Symp. San Diego, 1991), Vol. 1, IEEE, New York (1991) 1199.
[10] KIM, J., et al., Phys. Rev. Lett. **72** (1994) 2199.
[11] CARLSTROM, T., et al., Rev. Sci. Instrum. **59** (1988) 1063.
[12] CARLSTROM, T.N., et al., Rev. Sci. Instrum. **63** (1992) 4901.
[13] FONCK, R.J., et al., Phys. Rev. **29** (1984) 3288.
[14] HORTON, L.D., et al., in Plasma Physics and Controlled Nuclear Fusion Research 1992 (Proc. 14th Int. Conf. Würzburg, 1992), Vol. 1, IAEA, Vienna (1993) 423.
[15] HINTON, F.L., CHU, M.S., Nucl. Fusion **25** (1985) 345.
[16] WESSON, J., Tokamaks, Clarendon Press, Oxford (1987).

(Manuscript received 25 July 1994
Final manuscript received 21 December 1994)